

# A Modality-Tailored Graph Modeling Framework for Urban Region Representation via Contrastive Learning

Yaya Zhao<sup>a</sup>, Kaiqi Zhao<sup>b</sup>, Zixuan Tang<sup>a</sup>, Zhiyuan Liu<sup>a</sup>, Xiaoling Lu<sup>a,\*</sup> and Yalei Du<sup>c</sup>

<sup>a</sup>Center for Applied Statistics, School of Statistics, Innovation Platform, Renmin University of China

<sup>b</sup>Harbin Institute of Technology, Shenzhen

<sup>c</sup>Beijing Baixingkefu Network Technology Co., Ltd.

{zhaoyaya, 2021201741, 2023201970, xiaolinglu}@ruc.edu.cn,  
zhaokaiqi@hit.edu.cn, yaleidu@163.com

**Abstract.** Graph-based models have emerged as a powerful paradigm for modeling multimodal urban data and learning region representations for various downstream tasks. However, existing approaches face two major limitations. (1) They typically employ identical graph neural network architectures across all modalities, failing to capture modality-specific structures and characteristics. (2) During the fusion stage, they often neglect spatial heterogeneity by assuming that the aggregation weights of different modalities remain invariant across regions, resulting in suboptimal representations. To address these issues, we propose MTGRR, a modality-tailored graph modeling framework for urban region representation, built upon a multimodal dataset comprising point of interest (POI), taxi mobility, land use, road element, remote sensing, and street view images. (1) MTGRR categorizes modalities into two groups based on spatial density and data characteristics: aggregated-level and point-level modalities. For aggregated-level modalities, MTGRR employs a mixture-of-experts (MoE) graph architecture, where each modality is processed by a dedicated expert GNN to capture distinct modality-specific characteristics. For the point-level modality, a dual-level GNN is constructed to extract fine-grained visual semantic features. (2) To obtain effective region representations under spatial heterogeneity, a spatially-aware multimodal fusion mechanism is designed to dynamically infer region-specific modality fusion weights. Building on this graph modeling framework, MTGRR further employs a joint contrastive learning strategy that integrates region aggregated-level, point-level, and fusion-level objectives to optimize region representations. Experiments on two real-world datasets across six modalities and three tasks demonstrate that MTGRR consistently outperforms state-of-the-art baselines, validating its effectiveness.

## 1 Introduction

Graph-based models have demonstrated a strong ability to capture complex spatial dependencies and relational structures among urban regions. Recent works [14, 33, 36] have leveraged this capability to learn comprehensive urban region representations from diverse data modalities, including points of interest (POIs), taxi trajectories, land use, road elements, remote sensing imagery, and street-view images. By integrating these multimodal data sources, the resulting region

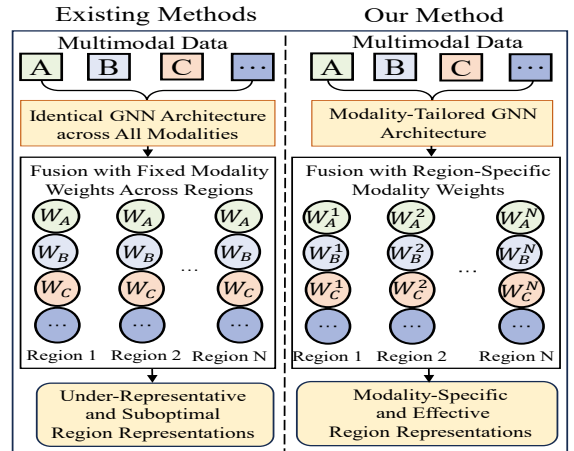


**Figure 1.** Comparison between existing methods and MTGRR.

representations capture the distinct semantic and structural characteristics of each modality. These representations can be applied to various downstream tasks, including carbon emission estimation [3], GDP prediction [15], and population forecasting [1].

Despite their effectiveness, existing graph-based models for urban region representation face two key limitations, as shown in Figure 1 (left). **Limitation 1:** Most approaches use identical graph neural network architectures across all modalities, applying uniform processing pipelines to heterogeneous data. For example, models such as [27, 36] integrate POI distributions and taxi mobility patterns, which represent different aspects of urban dynamics, yet they still process them using the same GCN architecture [9]. This modality-agnostic design leads to under-representative embeddings that fail to capture modality-specific structures and characteristics. **Limitation 2:** Existing modality fusion strategies often overlook spatial heterogeneity across regions, assuming that the contribution of each modality remains invariant across the city. For example, [33, 34] directly average modality outputs to obtain region representations, and the fusion weights are shared across regions, failing to capture region-specific modality importance. This results in suboptimal representations that fail to reflect spatially varying urban characteristics.

To address these issues, we propose **MTGRR**, a modality-tailored graph framework for urban region representation (Figure 1, right). It

\* Corresponding Author. Email: xiaolinglu@ruc.edu.cn.

leverages a comprehensive urban dataset comprising six modalities, categorized into two groups based on data characteristics and spatial density. (1) **Aggregated-level modalities** include POI, taxi mobility, land use, road element, and remote sensing imagery. Each POI is labeled with a functional category (e.g., restaurant, school); each taxi record is associated with a source region ID indicating inflow; each land parcel has a land-use label (e.g., residential, industrial); and each road segment is assigned a category label (e.g., living street, trunk link). For the first four modalities, modeling each point individually results in redundant information, as points with the same label exhibit highly similar features. Hence, they are better analyzed through label-based aggregation and treated as aggregated-level modalities. Although remote sensing imagery lacks explicit labels, it is considered aggregated-level because each region is associated with a single image that reflects region-level semantics. (2) **Point-level modality** refers to street-view imagery, where each region contains numerous images capturing fine-grained visual semantics at specific spatial locations. Due to significant variation among individual images and the absence of well-defined predefined labels for grouping, these data are modeled at the instance level and treated as a point-level modality.

Based on this modality classification, **MTGRR** constructs modality-tailored graph neural networks for the two distinct types of urban modalities. For aggregated-level modalities, MTGRR adopts a mixture-of-experts (MoE) graph architecture, which consists of a global heterogeneous graph integrating all modalities, a set of expert GNNs each dedicated to a specific modality, and a modality-aware gating mechanism that adaptively fuses expert outputs into distinct modality-specific representations. For the point-level modality (i.e., street-view imagery), MTGRR employs a dual-level graph neural network to extract fine-grained visual semantic features. All images are treated as first-level nodes, and a second-level virtual node is introduced per region to aggregate local features. Intra-region edges connect all first-level image nodes to their corresponding second-level virtual node, while inter-region connections are only established between second-level nodes of adjacent regions. This hierarchical design enhances localized visual semantic representations.

Furthermore, to obtain effective region representations under spatial heterogeneity, MTGRR introduces a spatially-aware multimodal fusion mechanism that dynamically learns region-specific fusion weights, allowing the model to adaptively adjust modality contributions across diverse regions and enhance the fused representations. Building on this framework, MTGRR adopts a joint contrastive learning strategy that integrates aggregated-level, point-level, and fusion-level objectives to optimize urban region representations.

- We propose **MTGRR**, a modality-tailored graph modeling framework for urban region representation, which constructs a mixture-of-experts (MoE) graph architecture for aggregated-level modalities and a dual-level graph neural network for the point-level modality, enabling effective extraction of modality-specific representations incorporating distinct modality characteristics.
- We introduce a spatially-aware multimodal fusion module that dynamically learns region-specific modality weights, enabling effective region representations that account for spatial heterogeneity.
- We design a joint contrastive learning strategy that integrates region aggregated-level, point-level, and fusion-level contrastive objectives, jointly optimizing multimodal region representations.
- We conduct extensive experiments on two real-world datasets covering six modalities and demonstrate that MTGRR consistently outperforms state-of-the-art methods across three downstream tasks, validating its effectiveness in diverse scenarios.

## 2 Related Work

**Graph Neural Networks for Multimodal Urban Data.** Graph Neural Networks (GNNs) have shown strong potential in modeling multimodal urban data [17], where heterogeneous sources such as POIs, taxi mobility, remote sensing, and street-view imagery are naturally structured as graphs. Recent works leverage GNNs to jointly encode semantic and spatial information across modalities. Early approaches often relied on single-modality data, such as taxi mobility, to define urban graphs [24, 25, 29], while more recent methods construct heterogeneous graphs from multiple modalities—e.g., [13, 27, 31, 36] combine POI and taxi mobility data to capture urban functionality and mobility patterns. Other studies [20] further incorporate land use or remote sensing imagery to model physical infrastructure and environmental context. Meanwhile, contrastive learning has emerged as an effective tool for enhancing graph-based representations [4, 12, 18]. Graph models [8, 33] has been adopted to align multi-view embeddings through contrastive objectives.

**Urban Region Representation Learning.** Urban region representation learning has gradually evolved from single-modality modeling to more sophisticated multimodal fusion frameworks. Early approaches primarily focused on individual data sources such as taxi mobility [25, 29], POIs [7], or satellite imagery [28], capturing only isolated aspects of urban dynamics. Recent studies increasingly incorporate multiple modalities to obtain richer and more comprehensive region representations [2, 10, 26, 32]. For example, Zhang et al. [32] propose a multi-view learning framework that combines taxi, POI, and check-in data to model regions from complementary perspectives. Multimodal fusion methods vary considerably in design. Some adopt general attention mechanisms [10, 19, 26], while others leverage graph-based structures to encode spatial correlations and relational dependencies [8, 31, 36]. In addition, recent models such as [35, 30] effectively integrate contrastive learning with multimodal fusion strategies to significantly enhance the quality and robustness of the learned region representations.

## 3 Preliminaries & Problem Statement

**Definition 1** (Urban Regions ( $\mathcal{U}$ )). *An urban area is partitioned into  $N$  non-overlapping regions, denoted as  $\mathcal{U} = \{U_1, U_2, \dots, U_N\}$ . Each  $U_i$  has a geographical boundary.*

**Definition 2** (Aggregated-Level Modalities). *A modality is defined as aggregated-level if each data point has a semantic label, and data points sharing the same label exhibit high feature similarity, making point-wise modeling redundant and better suited for label-based aggregation; or only one data instance exists per region, naturally representing region-level semantics.*

- **Point-of-Interest (POI) ( $\mathcal{P}$ ):** Each POI point is associated with a functional category label (e.g., restaurant, school). For each region  $U_i$ , the collection of POI data is denoted as  $P_i$ . Its feature vector is defined as  $P_{iV} = \{P_{i1}, P_{i2}, \dots, P_{i|\mathcal{P}|\}$ , where  $P_{ij}$  indicates the count of POIs in category  $j$  for region  $U_i$ .
- **Taxi Mobility ( $\mathcal{T}\mathcal{M}$ ):** Each taxi trip is associated with a source region label. For each region  $U_i$ , the collection of incoming taxi mobility flows is denoted as  $TM_i$ . Its feature vector is defined as  $TM_{iV} = \{TM_{i1}, TM_{i2}, \dots, TM_{iN}\}$ , where  $TM_{ij}$  indicates the number of trips arriving from region  $U_j$ .
- **Land Use ( $\mathcal{L}\mathcal{U}$ ):** Each land parcel is associated with a land use category label (e.g., residential, industrial). For each region  $U_i$ , the collection of land use data is denoted as  $LU_i$ . Its feature vector

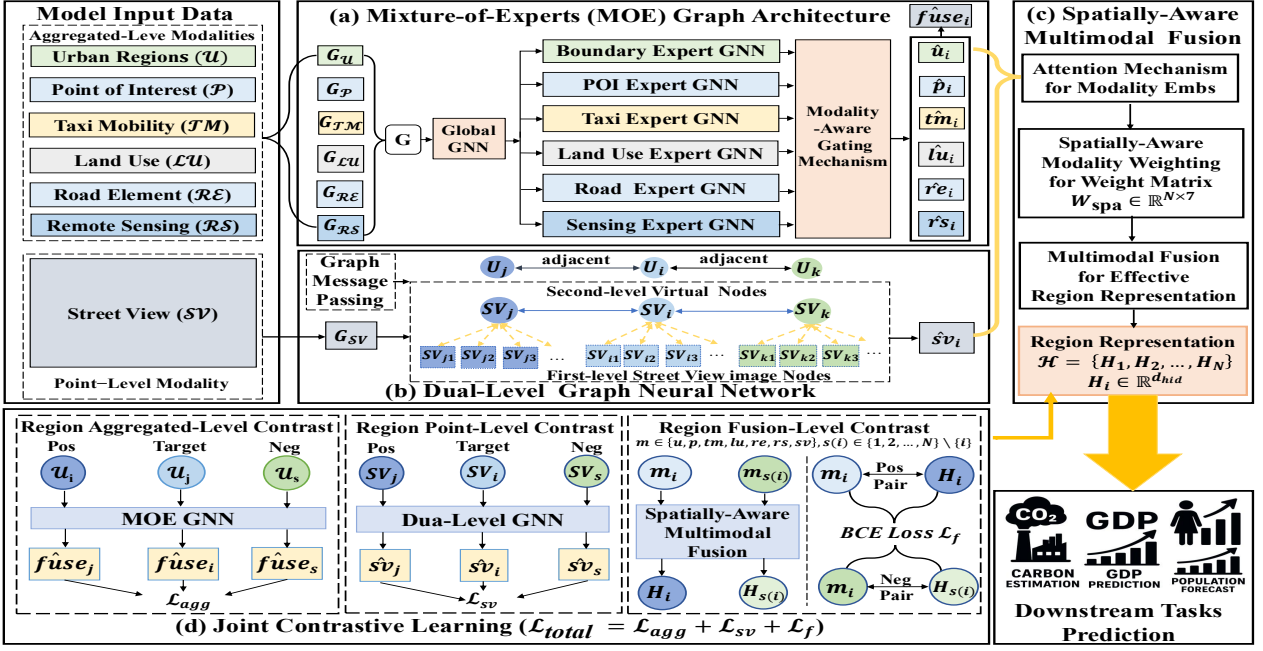


**Figure 2.** The framework: (a) MTGRR constructs a MoE graph architecture to model aggregated-level modalities, enabling distinct and accurate modality-specific representation. (b) A dual-level graph neural network is proposed to model the point-level street-view modality, capturing fine-grained visual semantic representations. (c) A spatially-aware fusion mechanism is introduced to dynamically infer region-specific modality fusion weights and generate effective region representations. (d) Region-level, point-level, and fusion-level contrastive objectives are jointly optimized for enhancing region representations.

is defined as  $LU_{-V_i} = \{LU_{i1}, LU_{i2}, \dots, LU_{i|\mathcal{L}U_i|\}$ , where  $LU_{ij}$  indicates the count of land parcels in category  $j$  for region  $U_i$ .

- **Road Element ( $\mathcal{RE}$ ):** Each road element has a road type label (e.g., trunk, motorway). For each region  $U_i$ , the collection of road element data is denoted as  $RE_i$ . Its feature vector is defined as  $RE_{-V_i} = \{RE_{i1}, RE_{i2}, \dots, RE_{i|\mathcal{R}E_i|\}$ , where  $RE_{ij}$  indicates the count of road elements in category  $j$  for region  $U_i$ .
- **Remote Sensing Imagery ( $\mathcal{RS}$ ):** For each region  $U_i$ , a remote sensing image is available and denoted as  $RS_i$ . Its feature vector  $RS_{-V_i} \in \mathbb{R}^{d_{in}}$  is extracted using an image encoder (e.g., EfficientNet-B4 [21]).

**Definition 3** (Point-Level Modality). A modality is defined as point-level if each region contains many data points with fine-grained spatial semantics, high feature variability, and no suitable labels for aggregation. It is thus better modeled at the point level.

- **Street View Imagery ( $\mathcal{SV}$ ):** Street-view images are abundant and unlabeled within each region, capturing fine-grained local appearances such as buildings and streetscapes. For each region  $U_i$ , a set of images  $\{SV_{i1}, SV_{i2}, \dots, SV_{i|\mathcal{S}V_i|\}$  is collected, where each  $SV_{ij}$  denotes the  $j$ -th street view image within region  $U_i$ .

**Definition 4** (Problem Statement: Urban Region Representation). Given urban regions  $\mathcal{U} = \{U_1, U_2, \dots, U_N\}$  associated with aggregated-level modalities  $\{\mathcal{P}, \mathcal{TM}, \mathcal{LU}, \mathcal{RE}, \mathcal{RS}\}$  and point-level modality  $\mathcal{SV}$ , the objective is to learn a low-dimensional embedding  $H_i \in \mathbb{R}^{d_{hid}}$  for each region  $U_i$ , resulting in embeddings  $\mathcal{H} = \{H_1, H_2, \dots, H_N\}$ . These embeddings are then used to predict  $K$  downstream tasks by applying a Ridge regression model, represented as  $Y \in \mathbb{R}^{N \times K}$ , which includes tasks such as carbon emission estimation, GDP prediction, and population forecasting.

## 4 Methodology

We propose **MTGRR** (Figure 2), a graph-based framework for urban region representation. (1) To address **Limitation 1**, MTGRR respectively designs tailored GNNs for aggregated-level and point-level modalities to capture modality-specific representations. (2) To address **Limitation 2**, it introduces a spatially-aware multimodal fusion mechanism to enable more effective region representations. (3) Finally, MTGRR employs a joint contrastive learning strategy to further optimize and enhance region representations.

### 4.1 Mixture-of-Experts (MoE) Graph Architecture

To learn distinct and accurate modality-specific representations for aggregated-level modalities, we design a MoE graph architecture.

#### 4.1.1 Global Heterogeneous Graph Neural Network

**Heterogeneous Graph Construction**  $G = (\mathcal{V}, \mathcal{E})$ . For each region  $U_i$ , according to Definition 2, it is associated with five region-aggregated modalities: a POI entity  $P_i$ , a taxi mobility entity  $TM_i$ , a land use entity  $LU_i$ , a road element entity  $RE_i$ , and a remote sensing entity  $RS_i$ . Each entity is represented by a feature vector, denoted as  $P_{-V_i}$ ,  $TM_{-V_i}$ ,  $LU_{-V_i}$ ,  $RE_{-V_i}$ , and  $RS_{-V_i}$ , respectively. Based on this information, we first construct six subgraphs as follows:

- **Region boundary graph  $G_U$ :** nodes  $\mathcal{V}_U = \{U_1, U_2, \dots, U_N\}$ , where each  $U_i$  represents a region. An edge  $(U_i, U_j) \in \mathcal{E}_U$  is created if regions  $U_i$  and  $U_j$  are geographically adjacent.
- **POI graph  $G_P$ :** nodes  $\mathcal{V}_P = \{P_1, P_2, \dots, P_N\}$ . An edge  $(P_i, P_j) \in \mathcal{E}_P$  is created if  $\text{cosine}(P_{-V_i}, P_{-V_j}) > \epsilon_P$ .
- **Taxi mobility graph  $G_{TM}$ :** nodes  $\mathcal{V}_{TM} = \{TM_1, TM_2, \dots, TM_N\}$ . An edge  $(TM_i, TM_j) \in \mathcal{E}_{TM}$  is created if  $\text{cosine}(TM_{-V_i}, TM_{-V_j}) > \epsilon_{TM}$ .

- **Land use graph**  $G_{\mathcal{L}U}$ : nodes  $\mathcal{V}_{\mathcal{L}U} = \{LU_1, LU_2, \dots, LU_N\}$ . An edge  $(LU_i, LU_j) \in \mathcal{E}_{\mathcal{L}U}$  is created if  $\text{cosine}(LU\_V_i, LU\_V_j) > \epsilon_{\mathcal{L}U}$ .
- **Road element graph**  $G_{\mathcal{R}E}$ : nodes  $\mathcal{V}_{\mathcal{R}E} = \{RE_1, RE_2, \dots, RE_N\}$ . An edge  $(RE_i, RE_j) \in \mathcal{E}_{\mathcal{R}E}$  is created if  $\text{cosine}(RE\_V_i, RE\_V_j) > \epsilon_{\mathcal{R}E}$ .
- **Remote sensing graph**  $G_{\mathcal{R}S}$ : nodes  $\mathcal{V}_{\mathcal{R}S} = \{RS_1, RS_2, \dots, RS_N\}$ . An edge  $(RS_i, RS_j) \in \mathcal{E}_{\mathcal{R}S}$  is created if  $\text{cosine}(RS\_V_i, RS\_V_j) > \epsilon_{\mathcal{R}S}$ .

Then, we build the final heterogeneous graph  $G = (\mathcal{V}, \mathcal{E})$  by integrating all nodes and edges from the six subgraphs and introducing cross-modality connections. Specifically, for each region  $U_i$  ( $i = 1, 2, \dots, N$ ), we add edges connecting  $U_i$  to its modality-specific nodes  $P_i, TM_i, LU_i, RE_i$ , and  $RS_i$  to enable information exchange across modalities.

**Global Graph Neural Network.** To capture cross-region and cross-modality interactions, we apply a global graph neural network over the heterogeneous graph  $G = (\mathcal{V}, \mathcal{E})$ . For each region boundary node  $U_i$ , POI node  $P_i$ , taxi mobility node  $TM_i$ , land use node  $LU_i$ , road element node  $RE_i$ , and remote sensing node  $RS_i$ , we randomly initialize their node representations as  $\mathbf{u}_i, \mathbf{p}_i, \mathbf{tm}_i, \mathbf{lu}_i, \mathbf{re}_i$ , and  $\mathbf{rs}_i$ , respectively, where all representations lie in  $\mathbb{R}^{d_{\text{in}}}$ . We use a multi-layer GAT model [23] to update node embeddings through message passing. After  $C$  layers, the updated embeddings are further refined via a feed-forward neural network FNN( $\cdot$ ) [22]. The final outputs for all modality-specific nodes are denoted as  $\{\bar{\mathbf{u}}_i, \bar{\mathbf{p}}_i, \bar{\mathbf{tm}}_i, \bar{\mathbf{lu}}_i, \bar{\mathbf{re}}_i, \bar{\mathbf{rs}}_i\}$ , where each vector lies in  $\mathbb{R}^{d_{\text{hid}}}$ .

#### 4.1.2 Dedicated Expert Graph Neural Network

Then, to extract the unique semantic characteristics of each modality, we construct a separate modality-specific expert graph neural network for each of the six subgraphs: a region boundary expert GNN for  $G_{\mathcal{U}}$ , a POI expert GNN for  $G_{\mathcal{P}}$ , a taxi mobility expert GNN for  $G_{\mathcal{T}M}$ , a land use expert GNN for  $G_{\mathcal{L}U}$ , a road element expert GNN for  $G_{\mathcal{R}E}$ , and a remote sensing expert GNN for  $G_{\mathcal{R}S}$ . Each expert GNN maintains its own parameters without sharing across modalities, allowing independent modeling of modality-specific structures.

Taking the POI expert GNN for  $G_{\mathcal{P}}$  as an example, the representation of node  $P_i$  at the  $l$ -th layer is denoted as  $\tilde{\mathbf{p}}_i^{(l)} \in \mathbb{R}^{d_{\text{hid}}}$ . The initial node features are set as  $\tilde{\mathbf{p}}_i^{(0)} = \bar{\mathbf{p}}_i$ , where  $\bar{\mathbf{p}}_i$  is the output of node  $P_i$  from the global heterogeneous graph neural network. The edge representation for modality  $\mathcal{P}$  at layer  $l$ , denoted as  $e_{\mathcal{P}}^{(l)} \in \mathbb{R}^{d_{\text{hid}}}$ , is randomly initialized. The update rules for the node and edge representations at the  $l$ -th layer of the POI expert GNN are as follows:

$$\begin{aligned} \tilde{\mathbf{p}}_i^{(l)} &= \sigma \left( \sum_{j \in \mathcal{N}_{\mathcal{P}}(i) \cup \{i\}} \frac{\mathbf{W}_{\mathcal{P}}^{(l)} \left( \tilde{\mathbf{p}}_j^{(l-1)} \circ e_{\mathcal{P}}^{(l-1)} \right)}{\sqrt{|\mathcal{N}_{\mathcal{P}}(i)| \cdot |\mathcal{N}_{\mathcal{P}}(j)|}} \right), \\ e_{\mathcal{P}}^{(l)} &= \mathbf{E}_{\mathcal{P}}^{(l)} e_{\mathcal{P}}^{(l-1)} + \mathbf{b}_{\mathcal{P}}^{(l)}, \end{aligned} \quad (1)$$

where  $\sigma(\cdot)$  denotes the activation function,  $\mathbf{W}_{\mathcal{P}}^{(l)} \in \mathbb{R}^{d_{\text{hid}} \times d_{\text{hid}}}$ ,  $\mathbf{E}_{\mathcal{P}}^{(l)} \in \mathbb{R}^{d_{\text{hid}} \times d_{\text{hid}}}$ , and  $\mathbf{b}_{\mathcal{P}}^{(l)} \in \mathbb{R}^{d_{\text{hid}}}$  are the learnable parameters for the POI expert GNN at the  $l$ -th layer,  $\mathcal{N}_{\mathcal{P}}(i)$  denotes the index set of neighbors of node  $P_i$  in  $G_{\mathcal{P}}$ , and  $\circ$  denotes element-wise multiplication. After  $L$  layers, the final output  $\tilde{\mathbf{p}}_i^{(L)}$  for the POI node  $P_i$  is represented as  $\tilde{\mathbf{p}}_i \in \mathbb{R}^{d_{\text{hid}}}$ . Similarly, the final outputs for each modality, computed using their corresponding expert GNNs, are denoted as  $\tilde{\mathbf{u}}_i, \tilde{\mathbf{p}}_i, \tilde{\mathbf{tm}}_i, \tilde{\mathbf{lu}}_i, \tilde{\mathbf{re}}_i$ , and  $\tilde{\mathbf{rs}}_i$ , respectively.

#### 4.1.3 Modality-Aware Gating Mechanism

To dynamically fuse the expert outputs into distinct and accurate modality-specific representations, we design a modality-aware gating mechanism based on the feature vectors of each modality.

According to Definition 2, each region boundary node  $U_i$  is associated with five aggregated-level modality nodes  $\{P_i, TM_i, LU_i, RE_i, RS_i\}$ , with corresponding feature vectors  $\{P\_V_i, TM\_V_i, LU\_V_i, RE\_V_i, RS\_V_i\}$ . In addition, the feature vector for  $U_i$ , denoted as  $U\_V_i$ , is initialized using Node2Vec embeddings [5]. These feature vectors are separately projected into vectors in  $\mathbb{R}^{d_{\text{hid}}}$  through modality-specific linear transformations.

The projected feature vectors are concatenated into a matrix  $\text{Concat}_V \in \mathbb{R}^{6 \times d_{\text{hid}}}$ , which is passed through a gating network followed by a softmax function to produce the gating weights across the six modalities for region  $U_i$ , denoted as  $\mathbf{g}_i \in \mathbb{R}^6$ . These gating weights are used to modulate the outputs from the expert GNNs:

$$\hat{\mathbf{m}}_i = g_{i,m} \cdot \tilde{\mathbf{m}}_i, \quad \text{for each } m \in \{u, p, tm, lu, re, rs\}, \quad (2)$$

where  $g_{i,m}$  is the gating weight for modality  $m$  in  $\mathbf{g}_i$ , and  $\tilde{\mathbf{m}}_i$  is the corresponding expert GNN output. The gated output  $\hat{\mathbf{m}}_i$  is obtained by scaling  $\tilde{\mathbf{m}}_i$  with  $g_{i,m}$ , and is regarded as the final modality-specific representation produced by the MoE architecture.

#### 4.2 Dual-Level Graph Neural Network

In this subsection, to obtain fine-grained visual semantic representations for the point-level street-view modality, we design a dual-level graph neural network.

##### 4.2.1 Dual-Level Street-View Graph Construction

According to Definition 3, each region  $U_i$  is associated with a set of street-view images  $\{SV_{i1}, SV_{i2}, \dots, SV_{i|\mathcal{S}V_i|}\}$ . To aggregate local street-view features, we introduce a virtual node  $SV_i$  for each region  $U_i$ . Based on all image and virtual nodes, we construct a dual-level street-view graph  $G_{\mathcal{S}V}$  for all regions as follows:

- **Nodes of the street-view graph**  $G_{\mathcal{S}V}$ : (1) **First-level nodes**: All street-view images  $SV_{ij}$  ( $i = 1, 2, \dots, N; j = 1, 2, \dots, |\mathcal{S}V_i|$ ) are treated as individual *first-level nodes*, where  $i$  denotes region  $U_i$  and  $j$  indexes its associated images. (2) **Second-level nodes**: All virtual nodes  $SV_i$  ( $i = 1, 2, \dots, N$ ) are treated as *second-level nodes*, capturing the aggregated region street-view features.
- **Edges of the street-view graph**  $G_{\mathcal{S}V}$ : (1) **Intra-region edges**: For each region  $U_i$  ( $i = 1, 2, \dots, N$ ), the virtual node  $SV_i$  is connected to all its associated street-view image nodes  $\{SV_{ij}\}$ , where  $j = 1, 2, \dots, |\mathcal{S}V_i|$ . (2) **Inter-region edges**: Two virtual nodes  $SV_i$  and  $SV_j$  are connected if their corresponding regions  $U_i$  and  $U_j$  are geographically adjacent.

##### 4.2.2 Graph Message Passing Mechanism

To capture both intra- and inter-region interactions, we design a message passing mechanism for  $G_{\mathcal{S}V}$ . (1) Due to the large number of first-level image nodes, directly involving them in inter-region message passing would lead to an explosion of inter-region edges, significantly increasing the complexity of message propagation. Therefore, inter-region message passing occurs only between second-level virtual nodes. (2) Intra-region message passing occurs between each second-level virtual node and all first-level image nodes within the same region, enabling the capture of fine-grained visual semantics.

At the  $l$ -th layer, the representations of the first-level image nodes  $SV_{ij}$  and the second-level virtual nodes  $SV_i$  are denoted as  $\hat{\mathbf{sv}}_{ij}^{(l)}$  and  $\hat{\mathbf{sv}}_i^{(l)}$ , respectively, each in  $\mathbb{R}^{d_{feat}}$ . The initial features  $\hat{\mathbf{sv}}_{ij}^{(0)}$  are extracted using the CLIP-ViT-B/32 encoder [16]. The initial feature of the second-level node  $\hat{\mathbf{sv}}_i^{(0)}$  is obtained by averaging  $\{\hat{\mathbf{sv}}_{ij}^{(0)}\}_{j=1}^{|SV_i|}$ .

Then at the  $l$ -th GNN layer, node features are updated as:

$$\begin{aligned}\hat{\mathbf{sv}}_{ij}^{(l)} &= \sigma \left( \mathbf{W}_{sv1}^{(l)} \hat{\mathbf{sv}}_i^{(l-1)} \right), \quad j = 1, 2, \dots, |SV_i|, \\ \hat{\mathbf{sv}}_i^{(l)} &= \sigma \left( \sum_{j=1}^{|SV_i|} \mathbf{W}_{sv2}^{(l)} \hat{\mathbf{sv}}_{ij}^{(l-1)} + \sum_{s \in \mathcal{N}_{SV}(i)} \mathbf{W}_{sv3}^{(l)} \hat{\mathbf{sv}}_s^{(l-1)} \right),\end{aligned}\quad (3)$$

where  $\sigma$  denotes the activation function.  $\mathbf{W}_{sv1}^{(l)}$ ,  $\mathbf{W}_{sv2}^{(l)}$ , and  $\mathbf{W}_{sv3}^{(l)}$  in  $\mathbb{R}^{d_{feat} \times d_{feat}}$  are learnable. After  $Z$  layers, the final output  $\hat{\mathbf{sv}}_i^{(l)}$  for the second-level virtual node  $SV_i$  is passed through a feed-forward network  $\text{FNN}(\cdot)$  [22] to obtain the final region-level street-view representation  $\hat{\mathbf{sv}}_i \in \mathbb{R}^{d_{hid}}$  for each region  $U_i$ , where  $i = 1, 2, \dots, N$ .

### 4.3 Spatially-Aware Multimodal Fusion Mechanism

To learn more effective region representations by considering spatial heterogeneity, we introduce a spatially-aware fusion mechanism that dynamically infers region-specific modality fusion weights.

**Attention Mechanism for Cross-Modal Interactions.** For each region  $U_i$ ,  $i = 1, 2, \dots, N$ , we use modality-specific embeddings  $\{\hat{\mathbf{u}}_i, \hat{\mathbf{p}}_i, \hat{\mathbf{tm}}_i, \hat{\mathbf{lu}}_i, \hat{\mathbf{re}}_i, \hat{\mathbf{rs}}_i, \hat{\mathbf{sv}}_i\}$  obtained from the previous section. These embeddings are concatenated and fed into a multi-head attention module [22] to model cross-modal interactions, producing unified modality embeddings  $\mathbf{H}^f \in \mathbb{R}^{N \times 7 \times d_{hid}}$ , where the second and third dimensions correspond to modality and hidden size.

**Spatially-Aware Modality Weighting.** To adaptively capture heterogeneity in modality contributions across diverse regions, we propose a dynamic spatially-aware weighting module that generates a region-specific modality weight matrix  $\mathbf{W}_{\text{spa}} \in \mathbb{R}^{N \times 7}$ , where each row corresponds to a region and each column to a modality.

Specifically, we first compute a region-level context vector  $\mathbf{C} \in \mathbb{R}^{N \times d_{hid}}$  by averaging the cross-modal embeddings  $\mathbf{H}^f$  across the modality dimension. This context vector is then passed through a lightweight gating network to generate attention scores as follows:

$$\mathbf{C} = \text{Average}(\mathbf{H}^f), \quad \mathbf{O} = \sigma(\mathbf{C} \mathbf{W}_1) \mathbf{W}_2^\top, \quad \mathbf{W}_{\text{spa}} = \text{Softmax}(\mathbf{O}), \quad (4)$$

$\mathbf{W}_1 \in \mathbb{R}^{d_{hid} \times d_{hid}}$  and  $\mathbf{W}_2 \in \mathbb{R}^{7 \times d_{hid}}$  are learnable parameters,  $\sigma(\cdot)$  is a nonlinear activation (e.g., sigmoid), and softmax is applied over the modality dimension to normalize weights per region.

**Multimodal Fusion for Effective Region Representation.** Based on the spatial weights  $\mathbf{W}_{\text{spa}}$ , we compute the final region representations via the following multimodal fusion process:

$$\begin{aligned}\mathbf{H}^w &= (\mathbf{W}_{\text{spa}} \odot \mathbf{H}^f) \mathbf{W}_{\text{proj}}, \quad \mathbf{H}^c = p_1 \mathbf{H}^w + p_2 \mathbf{H}^f, \\ \mathcal{H} &= \text{Average}(\mathbf{H}^c, \text{dim} = 1)\end{aligned}\quad (5)$$

where  $\odot$  denotes element-wise multiplication along the modality dimension,  $\mathbf{W}_{\text{proj}} \in \mathbb{R}^{d_{hid} \times d_{hid}}$  is learnable, and  $p_1, p_2$  are learnable parameters.  $\mathcal{H} = \{H_1, H_2, \dots, H_N\}$ , with each  $H_i \in \mathbb{R}^{d_{hid}}$ , serves as the final region representation for downstream tasks.

### 4.4 Joint Contrastive Learning

To effectively optimize multimodal region representations, we introduce a joint contrastive learning strategy that integrates region aggregated-level, point-level, and fusion-level contrastive objectives.

**Region Aggregated-Level Contrastive Learning.** To enhance the effectiveness of aggregated-level modality representations, we introduce a region aggregated-level contrastive learning objective.

Specifically, for each region  $U_i$ , we obtain embeddings  $\{\hat{\mathbf{u}}_i, \hat{\mathbf{p}}_i, \hat{\mathbf{tm}}_i, \hat{\mathbf{lu}}_i, \hat{\mathbf{re}}_i, \hat{\mathbf{rs}}_i, \hat{\mathbf{sv}}_i\}$  for the aggregated-level modalities, each in  $\mathbb{R}^{d_{hid}}$  in Subsection 4.1. These embeddings are concatenated and averaged to obtain a unified feature  $\hat{\mathbf{fuse}}_i \in \mathbb{R}^{d_{hid}}$ . Given each anchor  $\hat{\mathbf{fuse}}_i$ , we select a positive sample  $\hat{\mathbf{fuse}}_j$  from a geographically adjacent region  $U_j$ , and a negative sample  $\hat{\mathbf{fuse}}_s$  from a non-adjacent region  $U_s$ . The contrastive loss is defined as:

$$\mathcal{L}_{agg} = \max \left( \|\hat{\mathbf{fuse}}_i - \hat{\mathbf{fuse}}_j\|_2 - \|\hat{\mathbf{fuse}}_i - \hat{\mathbf{fuse}}_s\|_2 + \gamma, 0 \right), \quad (6)$$

where  $\gamma$  is a margin hyperparameter and  $\|\cdot\|_2$  denotes the L2 norm.

**Region Point-Level Contrastive Learning.** Similarly, to enhance the effectiveness of point-level street-view representations, we introduce a region point-level contrastive learning objective.

Specifically, for each region  $U_i$ , we obtain a street-view embedding  $\hat{\mathbf{sv}}_i \in \mathbb{R}^{d_{hid}}$  in Subsection 4.2. Given each anchor  $\hat{\mathbf{sv}}_i$ , a positive sample  $\hat{\mathbf{sv}}_j$  is selected from a geographically adjacent region  $U_j$ , and a negative sample  $\hat{\mathbf{sv}}_s$  from a non-adjacent region  $U_s$ . The region point-level contrastive loss is defined as:

$$\mathcal{L}_{sv} = \max \left( \|\hat{\mathbf{sv}}_i - \hat{\mathbf{sv}}_j\|_2 - \|\hat{\mathbf{sv}}_i - \hat{\mathbf{sv}}_s\|_2 + \gamma, 0 \right). \quad (7)$$

**Region Fusion-Level Contrastive Learning.** To enhance the quality of fused region representations, we introduce a fusion-level contrastive objective based on binary cross-entropy (BCE) loss.

For each region  $U_i$ , we obtain its fused representation  $\mathcal{H}_i \in \mathbb{R}^{d_{hid}}$  (Subsection 4.3) and modality-specific embedding  $\hat{\mathbf{m}}_i$  (Subsections 4.1 or 4.2), where  $i \in \{1, 2, \dots, N\}$  and  $m \in \mathcal{A} = \{\mathbf{u}, \mathbf{p}, \mathbf{tm}, \mathbf{lu}, \mathbf{re}, \mathbf{rs}, \mathbf{sv}\}$ . For each  $(i, m)$ , a *positive pair* ( $y = 1$ ) is formed by matching  $\hat{\mathbf{m}}_i$  with its corresponding  $\mathcal{H}_i$ , while a *negative pair* ( $y = 0$ ) is created by matching  $\hat{\mathbf{m}}_i$  with a randomly sampled  $\mathcal{H}_{s(i)}$  from a different region  $U_{s(i)}$ , where  $s(i) \in \{1, 2, \dots, N\} \setminus \{i\}$ . The fusion-level contrastive loss is defined as:

$$\mathcal{L}_f = - \sum_{i=1}^N \sum_{m \in \mathcal{A}} (\log \Phi([\hat{\mathbf{m}}_i, \mathcal{H}_i]) + \log(1 - \Phi([\hat{\mathbf{m}}_i, \mathcal{H}_{s(i)}]))) , \quad (8)$$

where  $\Phi(\cdot)$  is a shared matching function implemented via a learnable MLP followed by a sigmoid activation.

**Training.** The final joint objective function is defined as:

$$\mathcal{L}_{total} = \mathcal{L}_{agg} + \mathcal{L}_{sv} + \mathcal{L}_f. \quad (9)$$

This objective is used to optimize the entire modality-tailored graph modeling framework and obtain the final region representations.

## 5 Evaluation

### 5.1 Experimental Setup

**Datasets and Metrics.** We use two real-world urban datasets from Hangzhou and Shanghai. The Shanghai dataset is based on [30, 28], while the Hangzhou dataset is compiled by us. Each dataset covers a set of urban regions  $\mathcal{U}$ , with defined geographic boundaries. For each region, we collect six modalities: POI ( $\mathcal{P}$ ), taxi mobility ( $\mathcal{TM}$ ), land use ( $\mathcal{LU}$ ), road element ( $\mathcal{RN}$ ), remote sensing imagery ( $\mathcal{RS}$ ), and street-view imagery ( $\mathcal{SV}$ ). These datasets support three tasks: carbon emission estimation, GDP prediction, and population forecasting. Dataset statistics are summarized in Table 1. Performance is evaluated using Mean Absolute Error (MAE), Root Mean Squared Error (RMSE), and Coefficient of Determination ( $R^2$ ).

**Table 1.** Statistics of multimodal features and downstream tasks data across regions.

Dataset	Regions	POI	Taxi Mobility	Land Use	Road Element	Remote Sensing	Street View	Carbon	GDP	Pop
Hangzhou	193	229682	418592	3984	16461	193	17072	385245	13021211	2151372
Shanghai	251	421000	106776	3916	22727	251	21755	844779	55343700	6898623

**Table 2.** Performance comparison of baseline models across three tasks (carbon estimation, GDP prediction, and population forecasting) in two cities.  $\mathcal{M}_1$ – $\mathcal{M}_6$  represent different modality combinations, and **ALL** denotes using all modalities:  $\mathcal{M}_1 = (\mathcal{P}, \mathcal{T}\mathcal{M})$ ,  $\mathcal{M}_2 = (\mathcal{R}\mathcal{S}, \mathcal{S}\mathcal{V})$ ,  $\mathcal{M}_3 = (\mathcal{P}, \mathcal{T}\mathcal{M}, \mathcal{L}\mathcal{U})$ ,  $\mathcal{M}_4 = (\mathcal{P}, \mathcal{T}\mathcal{M}, \mathcal{R}\mathcal{N}, \mathcal{R}\mathcal{S})$ ,  $\mathcal{M}_5 = (\mathcal{P}, \mathcal{T}\mathcal{M}, \mathcal{R}\mathcal{S}, \mathcal{S}\mathcal{V})$ ,  $\mathcal{M}_6 = (\mathcal{P}, \mathcal{T}\mathcal{M}, \mathcal{L}\mathcal{U}, \mathcal{R}\mathcal{S}, \mathcal{S}\mathcal{V})$ , **ALL** =  $(\mathcal{P}, \mathcal{T}\mathcal{M}, \mathcal{L}\mathcal{U}, \mathcal{R}\mathcal{N}, \mathcal{R}\mathcal{S}, \mathcal{S}\mathcal{V})$ .

Model	$\mathcal{M}$	Hangzhou								Shanghai								Carbon				
		Carbon				GDP				Population				Carbon				GDP				
		MAE ↓	RMSE ↓	R2 ↑	MAE ↓	RMSE ↓	R2 ↑	MAE ↓	RMSE ↓	R2 ↑	MAE ↓	RMSE ↓	R2 ↑	MAE ↓	RMSE ↓	R2 ↑	MAE ↓	RMSE ↓	R2 ↑	MAE ↓	RMSE ↓	R2 ↑
GraphST[34]	$\mathcal{M}_1$	403.44	527.93	0.393	44619	62849	0.001	3338.2	3993.3	0.288	884.59	1167.36	0.291	119309	184082	0.251	6739.5	8241.9	0.365			
ReCP[11]	$\mathcal{M}_1$	433.45	542.22	0.360	43789	59496	0.105	3276.5	3949.6	0.304	869.39	1074.09	0.400	115505	157699	0.450	5706.0	7207.2	0.515			
HREP[36]	$\mathcal{M}_1$	340.72	434.12	0.590	37406	49575	0.378	2751.9	3445.6	0.470	629.97	849.28	0.625	95373	125970	0.649	4553.5	5945.6	0.670			
UrbanVLP[6]	$\mathcal{M}_2$	428.79	544.21	0.355	39286	55508	0.221	3614.6	4384.5	0.142	733.48	943.20	0.537	109638	168654	0.371	5753.5	7325.3	0.498			
HAFusion[19]	$\mathcal{M}_3$	406.06	525.56	0.398	38777	55164	0.230	3397.5	4167.9	0.225	699.75	917.77	0.562	89708	148511	0.512	5239.3	6739.2	0.576			
GURPP[8]	$\mathcal{M}_4$	299.84	383.90	0.679	27582	36957	0.655	2792.0	3446.1	0.470	720.08	949.27	0.531	96774	131216	0.619	6564.7	8131.1	0.382			
MuseCL[30]	$\mathcal{M}_5$	440.22	568.45	0.296	50108	66063	0.003	3040.7	3756.7	0.370	938.63	1209.08	0.239	131563	192362	0.182	7106.1	8736.5	0.287			
FlexiReg[20]	$\mathcal{M}_6$	302.63	406.25	0.641	31887	44345	0.503	2453.9	3175.6	0.550	658.72	922.96	0.557	91837	133342	0.607	5054.1	6300.2	0.629			
MTGRR	$\mathcal{M}_1$	126.16	175.21	0.933	19583	28799	0.790	1922.2	2507.5	0.719	537.22	769.01	0.692	69455	97073	0.792	4112.5	5320.2	0.735			
	$\mathcal{M}_2$	<b>107.53</b>	<b>151.82</b>	<b>0.950</b>	20950	28374	0.796	1813.2	2325.9	0.759	477.83	728.17	0.724	70275	97067	0.792	3957.4	5071.6	0.760			
	$\mathcal{M}_3$	136.11	199.92	0.913	21126	29909	0.774	1899.8	2493.7	0.722	477.57	695.31	0.748	78269	103425	0.764	4191.6	5361.0	0.731			
	$\mathcal{M}_4$	120.57	162.37	0.943	23737	34875	0.692	1851.4	2374.4	0.748	482.99	729.20	0.723	69317	98764	0.784	4258.6	5451.7	0.722			
	$\mathcal{M}_5$	140.63	186.38	0.924	19607	27258	0.812	1688.8	2206.5	0.783	455.69	691.21	0.751	67890	91492	0.815	4093.8	5314.2	0.736			
	$\mathcal{M}_6$	135.92	184.20	0.926	21901	30780	0.760	1835.2	2266.2	0.771	497.31	742.55	0.713	70974	94821	0.801	4016.1	5188.7	0.748			
	ALL	110.06	163.52	0.942	<b>16994</b>	<b>23060</b>	<b>0.866</b>	<b>1681.8</b>	<b>2089.8</b>	<b>0.805</b>	<b>448.94</b>	<b>671.20</b>	<b>0.766</b>	<b>59782</b>	<b>84871</b>	<b>0.841</b>	<b>3851.1</b>	<b>4923.3</b>	<b>0.773</b>			

**Table 3.** Performance evaluation of ablation experiments across three tasks (carbon estimation, GDP prediction, and population forecasting) in two cities.

Method	$\mathcal{M}$	Hangzhou								Shanghai								Carbon				
		Carbon				GDP				Population				Carbon				GDP				
		MAE ↓	RMSE ↓	R2 ↑	MAE ↓	RMSE ↓	R2 ↑	MAE ↓	RMSE ↓	R2 ↑	MAE ↓	RMSE ↓	R2 ↑	MAE ↓	RMSE ↓	R2 ↑	MAE ↓	RMSE ↓	R2 ↑	MAE ↓	RMSE ↓	R2 ↑
w/o MOE-GNN		180.65	230.43	0.884	22185	30124	0.771	1978.3	2438.7	0.735	559.79	781.22	0.682	88511	118284	0.691	4740.4	6075.9	0.655			
w/o DL-GNN		156.11	221.05	0.894	21517	28427	0.796	1927.8	2531.1	0.714	531.57	728.68	0.724	67107	88169	0.828	4469.9	5923.1	0.672			
w/o $\mathcal{S}\mathcal{V}$		124.84	167.63	0.939	23298	34783	0.694	1996.7	2486.1	0.724	473.53	711.73	0.736	72195	95197	0.800	4293.6	5682.0	0.698			
w/o SA-MF		155.43	209.15	0.905	25145	35275	0.685	1893.8	2398.6	0.743	457.21	740.19	0.715	73852	105153	0.756	4089.4	5188.2	0.748			
w/o $\mathcal{L}_{sv}$		129.46	179.81	0.930	22798	32941	0.726	2006.7	2616.4	0.694	478.96	694.16	0.749	70124	98117	0.787	4240.4	5307.9	0.737			
w/o $\mathcal{L}_f$		150.44	206.24	0.907	21118	29349	0.782	1841.1	2411.2	0.741	439.85	697.69	0.747	76225	104142	0.760	4067.0	5208.5	0.746			
MTGRR		<b>110.06</b>	<b>163.52</b>	<b>0.942</b>	<b>16994</b>	<b>23060</b>	<b>0.866</b>	<b>1681.8</b>	<b>2089.8</b>	<b>0.805</b>	<b>448.94</b>	<b>671.20</b>	<b>0.766</b>	<b>59782</b>	<b>84871</b>	<b>0.841</b>	<b>3851.1</b>	<b>4923.3</b>	<b>0.773</b>			

**Baselines.** To evaluate the performance of MTGRR, we compare it with eight strong baselines: (1) **GraphST** [34], a self-supervised spatiotemporal graph model; (2) **ReCP** [11], a framework for consistent multi-view representation learning; (3) **HREP** [36], which incorporates heterogeneous region embedding with prompt learning; (4) **UrbanVLP** [6], integrating satellite and street-view modalities via vision-language pretraining; (5) **HAFusion** [19], using a dual-feature attentive fusion module to learn higher-order correlations; (6) **GURPP** [8], a graph-based region pretraining and prompting framework; (7) **MuseCL** [30], a multi-semantic contrastive learning approach for region profiling; (8) **FlexiReg** [20], a flexible region encoder supporting adaptive formation and task-aware prompt learning.

**Parameter Settings.** All models are trained using the Adam optimizer (learning rate = 0.0001) for 300 epochs on both Hangzhou and Shanghai datasets. The contrastive margin  $\gamma$  is fixed at 2 for both region aggregated-level and point-level objectives. For each modality-specific subgraph (see Subsection 4.1.1), the edge threshold  $\epsilon$ —including  $\epsilon_{\mathcal{P}}$ ,  $\epsilon_{\mathcal{T}\mathcal{M}}$ ,  $\epsilon_{\mathcal{L}\mathcal{U}}$ ,  $\epsilon_{\mathcal{R}\mathcal{E}}$ ,  $\epsilon_{\mathcal{R}\mathcal{S}}$ —is set as the 64th highest intra-modality cosine similarity. The node embedding dimension  $d_{feat}$  of  $G_{\mathcal{S}\mathcal{V}}$  is set to 168, and the dual-level GNN uses one  $Z=1$  layer. Additional hyperparameters are analyzed in Section 5.4. Experiments are conducted on a server with an Intel® Xeon® Gold 6148 CPU (80 cores, 2.40 GHz) and a 24 GB NVIDIA RTX 4090 GPU.

## 5.2 Overall Performance

Table 2 summarizes the performance of MTGRR and eight strong baselines across three tasks in two cities. The baselines are evaluated under six modality combinations  $\mathcal{M}_1$ – $\mathcal{M}_6$ , each representing a subset of the full modality set **ALL**, as shown in the column headers of Table 2. We report MTGRR’s performance under each subset and the full modality setting. **(1) Modality-Specific Superiority:** For each modality combination  $\mathcal{M}_1$ – $\mathcal{M}_6$ , MTGRR consistently outperforms all baselines using the same subset across all tasks and cities, demonstrating the advantage of our modality-tailored graph modeling framework in learning modality-specific and effective representations. **(2) Strong Performance with Limited Modalities:** Even when using reduced modality combinations  $\mathcal{M}_1$ – $\mathcal{M}_6$ , which are subsets of the full modality set **ALL**, MTGRR achieves strong results, often surpassing baselines that use more input data. This demonstrates its ability to maintain high accuracy with limited information, making it suitable for real-world scenarios where collecting comprehensive multimodal data is impractical or cost-prohibitive. **(3) Scalability with More Modalities:** MTGRR achieves its best performance under the full modality setting (**ALL**) in most cases, confirming that incorporating more modalities consistently and significantly improves predictive performance. The model demonstrates strong scalability and is able to effectively exploit diverse and comple-

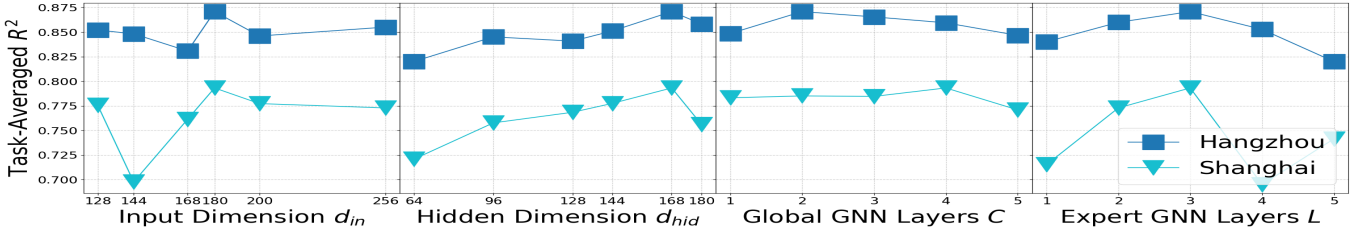


Figure 3. Hyperparameter study of MTGRR.

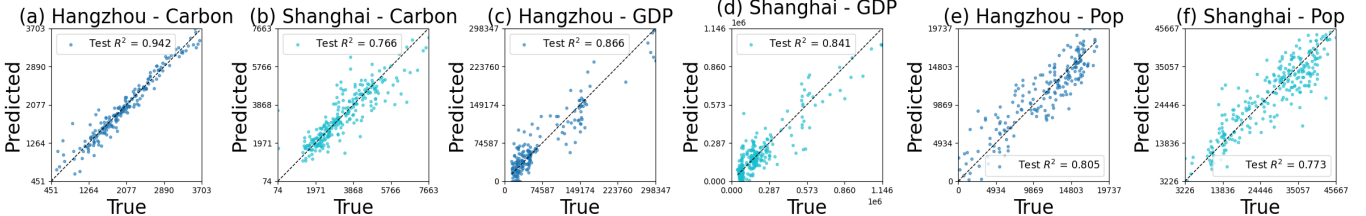


Figure 4. Predicted values generated by MTGRR versus ground truth on three downstream tasks across two cities.

mentary signals across modalities. **(4) Robustness Across Modality Combinations:** MTGRR maintains competitive performance across different modality combinations, tasks, and cities. This demonstrates its robustness in handling heterogeneous and incomplete modality inputs and its ability to flexibly adapt to diverse data distributions.

### 5.3 Ablation Study

To assess the contribution of each component in MTGRR, we design six ablation variants: (1) **w/o MOE-GNN**: Removes the expert GNNs and gating mechanism in the mixture-of-experts; each modality directly uses the output of the global GNN; (2) **w/o DL-GNN**: Removes all first-level street-view nodes and their message passing; only uses the second-level node averaged from them, which is processed by a GAT for final region representation. (3) **w/o SV**: Removes the street-view modality and all related modules; (4) **w/o SA-MF**: Removes the spatially-aware multimodal fusion mechanism and applies multi-head attention over all modality embeddings without spatial weighting; (5) **w/o  $\mathcal{L}_{sv}$** : Removes the point-level contrastive loss; (6) **w/o  $\mathcal{L}_f$** : Removes the fusion-level contrastive loss.

Table 3 shows that removing any individual component leads to performance degradation, confirming the importance of each module. Among all variants, **w/o MOE-GNN** and **w/o DL-GNN** result in the most significant drops, highlighting the critical role of our modality-tailored GNN designs for both aggregated and point-level modalities. Interestingly, **w/o DL-GNN** performs worse than **w/o SV**, indicating that applying a standard GNN to street-view data is less effective than removing it entirely—underscoring the necessity of dual-level modeling for point-level visual signals. In addition, **w/o SA-MF** also leads to notable degradation, validating the importance of spatially-aware fusion in learning effective region representations. Lastly, the performance drops observed in **w/o  $\mathcal{L}_{sv}$**  and **w/o  $\mathcal{L}_f$**  confirm the benefits of joint contrastive learning.

### 5.4 Hyperparameter Analysis

We analyze the effect of four key hyperparameters in MTGRR: the input dimension  $d_{in}$  for node representations in the global GNN, the hidden dimension  $d_{hid}$  of modality representations used in multimodal fusion, the number of global GNN layers  $C$ , and the number of expert GNN layers  $L$ . As shown in Figure 3, we report the average  $R^2$  across three prediction tasks—carbon emission, GDP, and population—in both Hangzhou and Shanghai. We observe that the best performance in both cities is consistently achieved with  $d_{in} = 180$ ,  $d_{hid} = 168$ , and  $L = 3$ . The optimal global GNN depth is  $C = 2$  for Hangzhou and  $C = 4$  for Shanghai.

### 5.5 Prediction Visualization and Fitting Ability

To further assess the prediction quality of MTGRR, we visualize the predicted values versus the ground truth for three downstream tasks—carbon emission, GDP, and population—in both Hangzhou and Shanghai, as shown in Figure 4. Each subplot corresponds to a specific city-task pair and reports the  $R^2$  score on the test set. We observe that the predicted values align closely with the ground truth, capturing both linear and nonlinear trends with high accuracy. The  $R^2$  scores exceed 0.75 across all tasks and cities, demonstrating that the learned region representations are highly effective for prediction.

## 6 Discussion and Conclusion

We propose **MTGRR**, a modality-tailored graph framework for urban region representation. It integrates specialized GNNs and a spatially-aware fusion mechanism, jointly optimized via contrastive learning to derive effective region representations for downstream prediction tasks. Experiments across cities and tasks validate its superior performance and robustness. In future work, we will explore architectures beyond GNNs, such as large language models (LLMs), to better capture multimodal dependencies, and consider optimization methods beyond contrastive learning, including generative and reinforcement learning, to further enhance region representations.

## Acknowledgments

This work is supported by the National Natural Science Foundation of China (No. 72171229), the MOE Project of the Key Research Institute of Humanities and Social Sciences (No. 22JJD110001), and the Big Data and Responsible Artificial Intelligence for National Governance at Renmin University of China. Yaya Zhao is supported by the "Qiushi Academic-Dongliang" Project of Renmin University of China (No. RUC24QSDL063).

## References

- [1] L. Chen, T. Mu, X. Li, and J. Dong. Population prediction of chinese prefecture-level cities based on multiple models. *Sustainability*, 2022. URL <https://api.semanticscholar.org/CorpusID:248303889>.
- [2] M. Chen, Z. Li, H. Jia, X. Shao, J. Zhao, Q. Gao, M. Yang, and Y. Yin. Mgrl4re: A multi-graph representation learning approach for urban region embedding. *ACM Trans. Intell. Syst. Technol.*, Jan. 2025. ISSN 2157-6904. doi: 10.1145/3712698. URL <https://doi.org/10.1145/3712698>.
- [3] D. Dai, B. Zhou, S. Zhao, K. Li, and Y. Liu. Research on industrial carbon emission prediction and resistance analysis based on cei-egm-rrm method: a case study of bengbu. *Scientific Reports*, 13(1):14528, 2023. doi: 10.1038/s41598-023-41857-0. URL <https://doi.org/10.1038/s41598-023-41857-0>.
- [4] L. Gong, Y. Lin, S. Guo, Y. Lin, T. Wang, E. Zheng, Z. Zhou, and H. Wan. Contrastive pre-training with adversarial perturbations for check-in sequence representation learning. *Proceedings of the AAAI Conference on Artificial Intelligence*, 37(4):4276–4283, Jun. 2023. doi: 10.1609/aaai.v37i4.25546. URL <https://ojs.aaai.org/index.php/AAAI/article/view/25546>.
- [5] A. Grover and J. Leskovec. node2vec: Scalable feature learning for networks. In *Proceedings of the 22nd ACM SIGKDD international conference on Knowledge discovery and data mining*, pages 855–864, 2016.
- [6] X. Hao, W. Chen, Y. Yan, S. Zhong, K. Wang, Q. Wen, and Y. Liang. Urbanvlp: Multi-granularity vision-language pretraining for urban socioeconomic indicator prediction. In *Proceedings of the AAAI Conference on Artificial Intelligence*, volume 39, pages 28061–28069, 2025. doi: 10.1609/aaai.v39i27.35024.
- [7] W. Huang, D. Zhang, G. Mai, X. Guo, and L. Cui. Learning urban region representations with pois and hierarchical graph infomax. *ISPRS Journal of Photogrammetry and Remote Sensing*, 196:134–145, 2023.
- [8] J. Jin, Y. Song, D. Kan, H. Zhu, X. Sun, Z. Li, X. Sun, and J. Zhang. Urban region pre-training and prompting: A graph-based approach. *arXiv preprint arXiv:2408.05920*, 2024.
- [9] T. N. Kipf and M. Welling. Semi-supervised classification with graph convolutional networks. In *International Conference on Learning Representations (ICLR)*, 2017.
- [10] Y. Li, W. Huang, G. Cong, H. Wang, and Z. Wang. Urban region representation learning with openstreetmap building footprints. In *Proceedings of the 29th ACM SIGKDD Conference on Knowledge Discovery and Data Mining*, pages 1363–1373, 2023.
- [11] Z. Li, W. Huang, K. Zhao, M. Yang, Y. Gong, and M. Chen. Urban region embedding via multi-view contrastive prediction. In *Proceedings of the AAAI Conference on Artificial Intelligence*, volume 38, pages 8724–8732, 2024.
- [12] Z. Long, L. Zhuang, G. Killick, Z. Meng, R. Mccreadie, and G. Aragon-Camarasa. Clce: An approach to refining cross-entropy and contrastive learning for optimized learning fusion. In *ECAI 2024*, pages 1800–1807. IOS Press, 2024.
- [13] Y. Luo, F.-l. Chung, and K. Chen. Urban region profiling via multi-graph representation learning. In *Proceedings of the 31st ACM international conference on information & knowledge management*, pages 4294–4298, 2022.
- [14] S. Mandal and N. E. O’Connor. Llmasmmkg: Llm assisted synthetic multi-modal knowledge graph creation for smart city cognitive digital twins. *Proceedings of the AAAI Symposium Series*, 4:210–221, 2024.
- [15] P. Perera and A. Fernando. Impact of energy prices and macroeconomic variables on gdp prediction uk: Machine learning approach. *Journal of Business and Management Studies*, 2024. URL <https://api.semanticscholar.org/CorpusID:273115300>.
- [16] A. Radford, J. W. Kim, C. Hallacy, A. Ramesh, G. Goh, S. Agarwal, G. Sastry, A. Askell, P. Mishkin, J. Clark, et al. Learning transferable visual models from natural language supervision. In *International conference on machine learning*, pages 8748–8763. PMLR, 2021.
- [17] M. Schlichtkrull, T. N. Kipf, P. Bloem, R. Van Den Berg, I. Titov, and M. Welling. Modeling relational data with graph convolutional networks. In *The semantic web: 15th international conference, ESWC 2018*, pages 593–607. Springer, 2018.
- [18] C. Shui, X. Li, J. Qi, G. Jiang, and Y. Yu. Hierarchical graph contrastive learning for review-enhanced recommendation. In A. Bifet, J. Davis, T. Kraljavičius, M. Kull, E. Ntoutsi, and I. Žliobaitė, editors, *Machine Learning and Knowledge Discovery in Databases. Research Track*, pages 423–440, Cham, 2024. Springer Nature Switzerland. ISBN 978-3-031-70365-2.
- [19] F. Sun, J. Qi, Y. Chang, X. Fan, S. Karunasekera, and E. Tanin. Urban region representation learning with attentive fusion. In *2024 IEEE 40th International Conference on Data Engineering (ICDE)*, pages 4409–4421. IEEE, 2024.
- [20] F. Sun, Y. Chang, E. Tanin, S. Karunasekera, and J. Qi. Urban region representation learning: A flexible approach, 2025. URL <https://arxiv.org/abs/2503.09128>.
- [21] M. Tan and Q. Le. Efficientnet: Rethinking model scaling for convolutional neural networks. In *International conference on machine learning*, pages 6105–6114. PMLR, 2019.
- [22] A. Vaswani, N. Shazeer, N. Parmar, J. Uszkoreit, L. Jones, A. N. Gomez, Ł. Kaiser, and I. Polosukhin. Attention is all you need. In *Advances in Neural Information Processing Systems (NeurIPS)*, pages 5998–6008, 2017.
- [23] P. Velickovic, G. Cucurull, A. Casanova, A. Romero, P. Liò, and Y. Bengio. Graph attention networks. In *Proceedings of the 6th International Conference on Learning Representations (ICLR)*, 2018.
- [24] H. Wang and Z. Li. Region representation learning via mobility flow. In *Proceedings of the 2017 ACM on Conference on Information and Knowledge Management*, pages 237–246, 2017.
- [25] S. Wu, X. Yan, X. Fan, S. Pan, S. Zhu, C. Zheng, M. Cheng, and C. Wang. Multi-graph fusion networks for urban region embedding. In *Proceedings of the Thirty-First International Joint Conference on Artificial Intelligence, IJCAI-22*, pages 2312–2318, 2022.
- [26] C. Xiao, J. Zhou, Y. Xiao, J. Huang, and H. Xiong. Refound: Crafting a foundation model for urban region understanding upon language and visual foundations. In *Proceedings of the 30th ACM SIGKDD Conference on Knowledge Discovery and Data Mining*, 2024. ISBN 9798400704901.
- [27] Z. Xu and X. Zhou. Cgap: Urban region representation learning with coarsened graph attention pooling. In K. Larson, editor, *Proceedings of the Thirty-Third International Joint Conference on Artificial Intelligence, IJCAI-24*, pages 7518–7526, 2024.
- [28] Y. Yan, H. Wen, S. Zhong, W. Chen, H. Chen, Q. Wen, R. Zimmermann, and Y. Liang. Urbanclip: Learning text-enhanced urban region profiling with contrastive language-image pretraining from the web. In *Proceedings of the ACM Web Conference 2024, WWW ’24*, page 4006–4017, 2024.
- [29] Z. Yao, Y. Fu, B. Liu, W. Hu, and H. Xiong. Representing urban functions through zone embedding with human mobility patterns. In *Proceedings of the Twenty-Seventh International Joint Conference on Artificial Intelligence (IJCAI-18)*, 2018.
- [30] X. Yong and X. Zhou. Musecl: Predicting urban socioeconomic indicators via multi-semantic contrastive learning. In K. Larson, editor, *Proceedings of the Thirty-Third International Joint Conference on Artificial Intelligence, IJCAI-24*, pages 7536–7544, 2024.
- [31] L. Zhang, C. Long, and G. Cong. Region embedding with intra and inter-view contrastive learning. *IEEE Transactions on Knowledge and Data Engineering*, 35(9):9031–9036, 2022.
- [32] M. Zhang, T. Li, Y. Li, and P. Hui. Multi-view joint graph representation learning for urban region embedding. In *Proceedings of the twenty-ninth international conference on international joint conferences on artificial intelligence*, pages 4431–4437, 2021.
- [33] Q. Zhang, C. Huang, L. Xia, Z. Wang, Z. Li, and S. Yiu. Automated spatio-temporal graph contrastive learning. In *Proceedings of the ACM Web Conference 2023*, pages 295–305, 2023.
- [34] Q. Zhang, C. Huang, L. Xia, Z. Wang, S. M. Yiu, and R. Han. Spatial-temporal graph learning with adversarial contrastive adaptation. In *International Conference on Machine Learning*, pages 41151–41163. PMLR, 2023.
- [35] Y. Zhang, Y. Fu, P. Wang, X. Li, and Y. Zheng. Unifying inter-region autocorrelation and intra-region structures for spatial embedding via collective adversarial learning. In *Proceedings of the 25th ACM SIGKDD International Conference on Knowledge Discovery & Data Mining*, pages 1700–1708, 2019.
- [36] S. Zhou, D. He, L. Chen, S. Shang, and P. Han. Heterogeneous region embedding with prompt learning. In *Proceedings of the AAAI Conference on Artificial Intelligence*, volume 37, pages 4981–4989, 2023.